NeuroImage: Clinical 21 (2019) 101592

Contents lists available at ScienceDirect

NeuroImage: Clinical

journal homepage: www.elsevier.com/locate/ynicl

An enriched granger causal model allowing variable static anatomical constraints

Kun Bi[a], Guoping Luo[a], Shui Tian[a], Siqi Zhang[a], Xiaoxue Liu[b], Qiang Wang[c], Qing Lu[a,*], Zhijian Yao[b,c,**]

[a] Key Laboratory of Child Development and Learning Science, School of Biological Sciences & Medical Engineering, Southeast University, Nanjing 210096, China
[b] Department of Psychiatry, Affiliated Nanjing Brain Hospital, Nanjing Medical University, Nanjing 210029, China
[c] Medical School of Nanjing University, Nanjing University, Nanjing 210093, China

ARTICLE INFO

Keywords:
Anatomical priors
Enriched granger causal model
Effective connectivity
MEG
Depression
DTI

ABSTRACT

The anatomical connectivity constrains but does not fully determine functional connectivity, especially when one explores into the dynamics over the course of a trial. Therefore, an enriched granger causal model (GCM) integrated with anatomical prior information is proposed in this study, to describe the dynamic effective connectivity to distinguish the depression and explore the pathogenesis of depression. In the proposed frame, the anatomical information was converted via an optimized transformation model, which was then integrated into the normal GCM by variational bayesian model. Magnetoencephalography (MEG) signals and diffusion tensor imaging (DTI) of 24 depressive patients and 24 matched controls were utilized for performance comparison. Together with the sliding windowed MEG signals under sad facial stimuli, the enriched GCM was applied to calculate the regional-pair dynamic effective connectivity, which were repeatedly sifted via feature selection and fed into different classifiers. From the aspects of model errors and recognition accuracy rates, results supported the superiority of the enriched GCM with anatomical priors over the normal GCM. For the effective connectivity with anatomical priors, the best subject discrimination accuracy of SVM was 85.42% (the sensitivity was 87.50% and the specificity was 83.33%). Furthermore, discriminative feature analysis suggested that the enriched GCM that detect the variable anatomical constraint on function could better detect more stringent and less dynamic brain function in depression. The proposed approach is valuable in dynamic functional dysfunction exploration in depression and could be useful for depression recognition.

1. Introduction

The human brain is a complex network of structurally and functionally interconnected regions. How anatomical connectivity constrains dynamic effective connectivity is under exploration, which could also help to recognize abnormal dynamics and predict mental disorders.

Along with the advances in the neuroimaging techniques and multimodal imaging analyses, researchers had introduced some conception and had much exploration about the combination of function and structure (Zhang et al., 2011; Dyrba et al., 2015; Henson et al., 2016; Vecchio et al., 2016; Ruddy et al., 2017; Zhigalov et al., 2017). The functional connectivity represented temporal coherence of brain regions, and anatomical connectivity measured anatomical integrity of white matter tracts, the material backbone for communication between brain regions (Catani et al., 2002). The anatomical connectivity data was used to simulate the brain function and explored how network structure produces functional neural activity (Honey et al., 2007). Polysynaptic structural connections enabled functional connections (Stephan et al., 2009) and functional connectivity reflected a dynamical process taking place on anatomical connectivity (Pereda et al., 2005), which resulted in a complex relationship between functional and anatomical connectivity (Stephan et al., 2009). The susceptible-infected-susceptible model was used to discovery that functional relations between nodes of a realistic anatomical network display clear patterns (Stam et al., 2016). Conversely, functional connectivity exerted effects on anatomical connectivity through mechanisms of plasticity (Hagmann et al., 2010). The structural networks constrained dynamical processes and functional processes might shape the underlying structure in their turn (Shew and Plenz, 2013). Although

* Corresponding author.
** Corresponding author at: Department of Psychiatry, Affiliated Nanjing Brain Hospital, Nanjing Medical University, Nanjing 210029, China
E-mail addresses: luq@seu.edu.cn (Q. Lu), zjyao@njmu.edu.cn (Z. Yao).

https://doi.org/10.1016/j.nicl.2018.11.002
Received 8 February 2018; Received in revised form 8 October 2018; Accepted 3 November 2018
Available online 05 November 2018

anatomical and effective connectivity were integrated to a certain extent, a better method of anatomical-effective integration could help to predict how changes in brain network structure can give rise to abnormal dynamics and disease (Kaiser, 2013; van Dellen et al., 2013; Meng et al., 2017).

Studies had found that the function-structure relations could be reconfigured under physiological (Hagmann et al., 2010; Sui et al., 2014), or pathological states (Zhang et al., 2011; Cocchi et al., 2014). The multimodal combination achieved higher prediction accuracy and enabled individualized prediction on multiple clinical measures in psychiatry (Meng et al., 2017), including depression (Sui et al., 2014). When processing negative stimuli, aberrant structural and functional networks were reported in subcortical area in depression (Wong et al., 2016). Both decreased functional and structural connectivity were showed between default mode network and cingulo-opercular network in depression (Yin et al., 2016). Depression patients had significant lower fractional anisotropy (FA) values in the fornix, as well as decreased functional connectivity in PFC (Geng et al., 2016). In our previous MEG study, the depression could be recognized by functional-structural coupling when the functional connectivity increased rapidly between salience network and ventral attention network via a dynamic change point detection strategy (Bi et al., 2016). Those emerged studies supported the fact that quantification of the disrupted dynamics might help better understand the cause of disorder, more targeted drug treatment, and diagnostic or prognostic indicators (Cribben et al., 2012; Hutchison et al., 2013) However, there is still no model about how detailed quantitative knowledge of anatomical connectivity affecting the dynamic functional/effective connectivity in depression.

Some abnormal effective connectivities were found in depression. (Musgrove et al., 2015; Li et al., 2017; Zheng et al., 2017; Geng et al., 2018; Kandilarova et al., 2018; Rolls et al., 2018). The granger causal model (GCM) and dynamic causal model (DCM) were the most popular methods to investigate the depression in MEG. In our previous MEG study, the Granger causality model was used to identify the depression patients and achieved high accuracy (Lu et al., 2013a, 2013b). Another previous MEG study using DCM showed that the effective connectivity from the dorsolateral prefrontal cortex (DLPFC) to the amygdala was greatly impaired and the effective connectivity from the amygdala to the anterior cingulate cortex (ACC) as well as effective connectivity from ACC to DLPFC was significantly increased (Lu et al., 2012). In an MEG study for ketamine-mediated response, MDD subjects showed enhanced connectivity estimates in backward connections, and controls showing enhanced connectivity estimates in forward connections by DCM (Gilbert et al., 2018). However, how the anatomical prior affects the effective connectivity for depression in MEG remains to be explored.

In this study, an enriched GCM integrated with anatomical prior information was presented to calculate the dynamic effective connectivity between core emotional regions under sad emotional facial stimuli and MEG scanning, in order to distinguish the depression. The amygdala, dorsolateral prefrontal cortex (DLPFC) and anterior cingulate cortex (ACC) were selected as the core emotional regions. The GCM was used for effective connectivity analysis between regions and was on data driven, which less affected by the hypothesis of physiological model. The anatomical connectivity that provided by tractography was constructed on DTI data as prior information. A transformation model was designed to convert the anatomical priors in a form of parameters in the enriched GCM. Together with the sliding windows over regional signals, the enriched GCM with the anatomical priors was applied to calculate the regional-pair dynamic effective connectivities, which were fed into classifiers for depression recognition. Furthermore, the anatomical connectivity and effective connectivity calculated by the normal GCM without anatomical priors were utilized for depression recognition separately as a performance comparison.

2. Methods and materials

2.1. Subjects

Twenty-four right-handed depression subjects (12 females) with an age range of 20–45 (mean, 33.2 ± 9.0 years) and educational level range of 10–18 (mean, 13.4 ± 2.5 years) were recruited from in-patient facilities at the Brain Hospital affiliated with Nanjing Medical University. The Brief Psychiatric Rating Scale (BPRS), the Structured Clinical Interview for the Diagnostic and Statistical Manual of Mental Disorders-IV (SCID) and the Hamilton Depressive Rating Scale (HDRS) were included in the eligibility screening procedures. The initial diagnoses of depression was made by the participants' treating psychiatrists and confirmed by an expert psychiatrist according to SCID. Depression subjects were included with HRDS scores > 21 on the day of scanning. Patients without other psychiatric illnesses were enrolled and currently taking no medications.

Twenty-four healthy control participants matched in gender (12 females), age (range of 21–44, mean, 31.8 ± 7.7 years) and educational level (range of 12–18, mean, 14.5 ± 2.0 years) participated in this study. They all didn't have any psychiatric illness presently or a history of psychiatric illness.

All subjects were satisfied the criteria to undergo a MEG scan. The study was approved by the Research Ethics Review Committee of the Brain Hospital affiliated with Nanjing Medical University. Written informed consents were obtained from all subjects. The demographic information for all subjects was provided in Table 1.

2.2. Sad facial affect recognition task and data acquisition

A facial expression paradigm was undertaken in this study. A series pictures were utilized to evoke stronger activity contrast. The emotional pictures included three conditions, neutral, sad and rest, where a fixation cross was displayed. Each condition had 40 trials and each lasted for 3 s, followed by a blank screen during the variable stimulus interval of 0.5 s, 1 s or 1.5 s. When scanned, the subjects were asked to identify whether the stimuli was sad or not by right hand click.

MEG data was recorded at a sampling rate of 1200 Hz using an Omega 2000 device of 275 channels placed in a magnetically shielded room (MSR), which provided a considerable amount of shielding from noise and interference.

DTI data and T1-weighted axial images were acquired using a Siemens Verio 3 T MRI scanner. The parameters for T1-weighted axial images were repetition time/echo time (TR/TE) =1900/2.48 ms, thickness/gap = 1.0/0 mm, matrix = 256 × 256 × 192, field of view (FOV) = 240 × 240 mm^2, voxel size = 1 × 1 × 1 mm^3. The following parameters were used for DTI scans, diffusion was measured along 30 non-collinear directions (b value = 1000s/mm^2), TR/TE = 6600 ms/

Table 1
Demographic and clinical characteristics of the subjects.[a]

Variables	Depression	HC	*P*-value
Sample size	24	24	–
Gender(male/female)	12/12	12/12	$P > 0.999$[b]
Age(years)	20–45(33.2 ± 9.0)	21–44(31.8 ± 7.7)	0.327[c]
Education(years)	10–18(13.4 ± 2.5)	12–18(14.5 ± 2.0)	0.114[c]
Handedness(right/left)	24/0	24/0	–
Score of 17-item HDRS	28.40 ± 3.75	–	–
Number of previous episodes	1.38 ± 0.64	–	–
Duration of illness (months)	4.04 ± 2.09	–	–

[a] Data were presented as the range of minimum-maximum (mean ± SD). HC = healthy controls.
[b] The *P* value was obtained by two-tailed Pearson chi-square test.
[c] The *P* value was obtained by two-sample two-tailed *t*-test.

93 ms, FOV = 240 mm × 240 mm, Matrix = 128 × 128 × 45, voxel size = 1.875 × 1.875 × 3 mm^3.

2.3. MEG and DTI data preprocessing

The MEG data were preprocessed with the SPM8 toolbox (www.fil.ion.ucl.ac.uk/spm). We divided the MEG recording into epochs from -100 ms to 900 ms. The interval from −100 ms to 0 ms was used for a baseline correction. The data were band-pass filtered from 1 to 48 Hz. Artifact detection was taken with a threshold of 2×10^{-12} Tesla for all channels. None was marked as bad channel and excluded from further analysis since < 10% trials were detected as artifacts. Finally, the trials under sad stimuli were averaged for each participant. Distributed source reconstruction of MEG data was via SPM8. The subjects' T1-weighted MRIs were segmented and the linear transformation matrices from individual anatomical space to the template space were calculated. The minimum-norm estimation algorithm was selected in the source reconstruction (Dale et al., 2000; Jensen and Hesse, 2010) and the evoked activity for each voxel was extracted.

DTI preprocessing was computed using FMRIB's Diffusion Toolbox (FSL, http://www.fmrib.ox.ac.uk/fsl/fdt/index.html). The eddy current distortions and motion artifacts were corrected by applying a rigid-body transformation of each diffusion-weighted image to the b0 image. To enable group comparison, the diffusion images were registered to MNI-152 space using a 12-parameter affine transform (Jenkinson et al., 2002). Diffusion toolkit (http://www.trackvis.org) toolbox was employed for fiber tract reconstruction. 30 fibers were initiated in a voxel (Cheng et al., 2012). The starting points were chosen spatially at random within the voxel where the FA value was > 0.3 (Thottakara et al., 2006). The tracking procedure was terminated at voxels with an FA value of < 0.15 or when the angle between adjacent steps was > 45° (Thottakara et al., 2006).

2.4. Regions of interest selection

Brain imaging studies in depression have proved that abnormalities in prefrontal-limbic circuit, particularly in the amygdala, ACC and DLPFC, were closely associated with dysfunctions of emotion processing (Davidson et al., 2002; Wackerhagen et al., 2017). It could be a good explanation that the DLPFC was critically engaged in cognitive regulation of emotion, and the ACC was a bridge between emotion and attention, particularly the amygdala was a core structure for automatic appraisal and emotion generation (Davidson et al., 2002; Klumpp et al., 2017).

As a result, we defined these three emotional regions of interest (ROIs), including the amygdala, DLPFC and ACC for further study. Anatomical ROIs masks were obtained from the Anatomical Automated Labeling (AAL) library for above three regions in the Marsbar toolbox (http://marsbar.sourceforge.net/).

2.5. Enriched effective connectivity with anatomical information

An enriched GCM integrated with anatomical prior information was presented to calculate the effective connectivity. The multivariate autoregressive (MAR) model in normal GCM was optimized by anatomical priors to establish the enriched GCM to investigate the effective connectivity. The anatomical connectivity that provided by tractography was constructed on DTI data as prior information. The enriched GCM with the static anatomical priors was applied to calculate the regional-pair effective connectivity.

2.5.1. Enriched GCM via a variational bayesian model

According to the definition of normal conditional GCM (Granger, 1969; Granger, 1980), in the multi-variable system, variables X_1, $X_2, \cdots X_n$satisfied certain conditions. Variable X_1 granger caused variable, if the value of variable predicted with X_1, $X_2, \cdots X_n$was better than the prediction of variableX_1, $X_3, \cdots X_n$. Moreover, conditional GCM could be measured that the influence of X_1 on X_2 was tested in the context of multiple additional variablesX_3, X_4, ⋯, X_n. The stationary time series$X_1(t)$, $X_2(t)$, $\cdots X_n(t)$ could be modeled as:

$$X_i(t) = \sum_{j=1}^{n} \sum_{k=1}^{p} A_{ij}(k) X_j(t-k) + \varepsilon_i(t) \tag{1}$$

Where p was the order of the model, A was the MAR coefficient matrix and $\varepsilon_i(t)$ (i = 1,2, …,n) was additive Gaussian noise with zero mean.

If $X_q(t)$was removed, the time series $X_m(t)$ which was predicted with other time series could also be modeled via:

$$X_m(t) = \sum_{j=1, j\neq q}^{n} \sum_{k=1}^{p} B_{mj}(k) X_j(t-k) + \eta_m(t) \tag{2}$$

B was the multivariate autoregressive (MAR) coefficient matrix and η_m(k) was additive Gaussian noise with zero mean. Hence, the influence of conditional granger causality from $X_q(t)$ to $X_m(t)$ could be defined as:

$$F_{X_q \to X_m | X_1, \cdots, X_n} = \ln \frac{\mathrm{var}(\eta_m)}{\mathrm{var}(\varepsilon_n)} \tag{3}$$

The MAR model of GCM in (1) and (2) could be simplified to the linear form of $Y = XW + E$ to investigate whether one time series X could correctly forecast another Y. W was the coefficient matrix of the MAR model and under further optimization; E was the zero-mean gaussian white noise with precision matrixΛ. Since the anatomical connectivity constrains but does not determine effective connectivity, a variational bayesian model (Roberts and Penny, 2002) was integrated into above normal GCM to construct an enriched GCM with anatomical priors. This allows different data points to be associated with different noise levels and effectively provides robust estimation of MAR coefficients. The variational bayesian model is used to prevent over-fitting and provides model-order selection criteria. Coefficient matrix W was transformed into a vector$w$, which obeyed a gauss distribution$N(0, \Sigma_{ij} = \alpha_{ij}^{-1})$. The anatomical connectivity information and the prior probability variance of GCM parameter w were connected by the following transformation model (Stephan et al., 2009).

$$\Sigma_{ij} = \frac{\Sigma_0}{1 + \Sigma_0 e^{b - c s_{ij}}} = \alpha_{ij}^{-1} = \frac{1}{\alpha_0 + e^{b - c s_{ij}}} \tag{4}$$

Among them, s_{ij} was the normalized anatomical connectivity between region i and j, Σ_0,b, $c$were the adjustable parameters of the model that would be optimized in the follow-up bayesian learning, in order to reasonably reflect how the anatomical connectivity partly constrained the effective connectivity.

A generic formulation was used to model a variety of different relationships between the likelihood of anatomical connectivity and the prior variance of the coefficient matrix W. The different transformation models were compared and selected by the criterion of negative free-energy.

2.5.2. Anatomical connectivity and transformation model

The anatomical connectivity was calculated between any two regions. (The details were shown in supplementary 1.1) As the effective connectivity was constrained by the anatomical connectivity to a certain extent, the anatomical connectivity was used to design the parameters of GCM by a transformation model. A series of anatomical transformation models were designed, each containing a different mathematical mapping between the anatomical connectivity s_{ij} and the prior variance Σ_{ij} of the GCM parameter w (Stephan et al., 2009) in the form of (4). The larger prior variance Σ_{ij} might reflect a larger variation range of the corresponding effective connectivity, which caused by increased anatomical connectivity. On the contrary, smaller prior variance Σ_{ij} might mean smaller variation range of the effective connectivity that caused by decreased anatomical connectivity. The

transformation model was established to describe the relationship between anatomical connectivity and parameters of the enriched GCM.

The best transformation model was selected by the largest negative free-energy $F(\theta)$with the change of parametersΣ_0,b, c in section 2.5.3. We fixed the upper bound hyperparameter Σ_0 to unity and optimize the remaining hyperparameters with respect to the model evidence by searching over the model space, where each model had different values of b and c.

2.5.3. Parameter optimization within the enriched GCM

The $\theta = \{w, \alpha, \Lambda\}$ was optimized by anatomical priors and solved by an algorithm like Expectation-Maximization algorithm (Moon, 1996). Any two parameters of θ were fixed to regulate the rest parameter and made $F(\theta)$ maximum, and the steps were repeated for all permutations of parameters. The iterations of these steps were continued until the optimization of the model was converged. The iterated steps of the algorithm were showed in supplementary 1.3.

2.6. Discriminative analysis with connectivity information

The time series of ROIs that selected in section 2.4 were extracted and principal component analysis (PCA) was performed independently for dimensionality reduction, ensuring that > 95% signal information was retained. Then, the time series of each region were separated via sequential time windows of 100 ms each with 20 ms overlap from 0 to 900 ms. For the normal GCM and enriched GCM, each subject had an $M \times N$ effective connectivity matrix, the number of sliding window M was 41 and the number of effective connectivity in one window N was 6. So each subject had 246 effective connectivity with anatomical prior, 246 effective connectivity without anatomical prior and 3 anatomical connectivity.

Within each time window of each subject, the orders of MAR model p for the enriched GCM were selected by the bayesian information criterion (BIC) and the akaike information criterion (AIC). The Fisher's z-values transformation was applied on the calculated effective connectivity and then a temporal effective connectivity matrix over regions was achieved to discriminate the depression from the healthy.

Features of connectivity were repeatedly sifted via minimum redundancy-maximum relevance (mRMR) feature selection algorithm (Ding and Peng, 2005) to reduce the dimension. The mRMR reduced mutual redundancy and determined maximum relevance within the features. The concept of mutual information defined the relevance and redundancy of the features. The computational cost was reduced by dimension reduction and the classification accuracy was improved by noise reduction. Then, the mRMR selected features were fed into the classifier for depression recognition. All the procedures of feature selection and classification were integrated in a leave-one-out cross validation scheme. The support vector machine (SVM), k-Nearest Neighbor (KNN), Nearest Mean Classifier (NMC), Linear Discriminate Analysis (LDA), Naïve Bayes Classifier (NBC) and Logistic Regression (LR) in the toolbox of PRtools (http://prtools.org/) were applied for performance comparison separately.

In order to investigate whether the enriched GCM is improved by the anatomical connectivity, the calculation with the sliding windows and discriminative analysis were repeated again for the effective connectivity without anatomical priors. Meanwhile, the discriminative analysis was repeated again for anatomical connectivity to estimate the influence of anatomical connectivity for depression recognition.

The normal vector of the classification hyperplane in SVM was used to analysis the contribution rates of discriminating elements. A permutation test was performed to compute the significance of these contribution rates. The original weights of discriminating features were computed for the original group labeling. For each resampling, the group labels were randomly rearranged and the weights were re-computed for the permuted data. The random rearrangement of group labels was repeated until a predefined number of resampling had been performed. The hypothesis was accepted or rejected based on the proportion of permuted weights equal to or greater than the original. Using the real sample label, the discriminating vectors highlighted that the effective connectivity showed the most distinctive characteristics between depression patients and healthy controls.

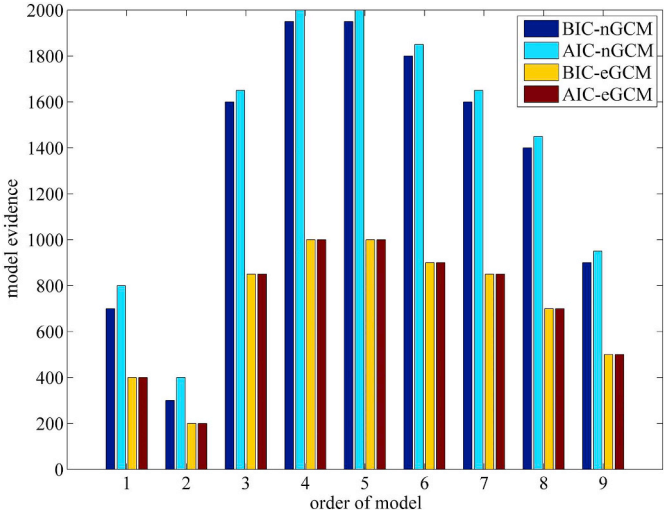

Fig. 1. Model evidence values for the enriched GCM with anatomical priors and normal GCM along with the variation of the model order. From left to right, four different colors represented BIC values of the normal GCM (BIC-nGCM), AIC values of the normal GCM (AIC-nGCM), BIC values of the enriched GCM (BIC-eGCM) and AIC values of the enriched GCM (AIC-eGCM).

3. Results

3.1. The selection of transformation models and the comparison between normal GCM and enriched GCM

With the largest negative free-energy value, model 53 illustrated in Fig. 1(b) was selected, where b = 4, c = 12 (The details were shown in supplementary 2). The order of multivariate autoregressive model p for GCMs was selected by model evidence. The model evidence was defined by the values of BIC and AIC together. As shown in Fig. 1, the model evidence of GCMs reached minimal when the model order p was set as two. The model evidence of enriched GCM with anatomical priors was significantly smaller than that of the normal GCM, suggesting that the model error of the enriched GCM with anatomical priors was significantly small.

3.2. Discriminative analysis

Using the regional-pair dynamic functional connectivity proposed as above, different classifiers together with feature selection of an mRMR framework were applied to predict the patients with depression. The discriminative analysis was repeated for the model of anatomical connectivity and two models of effective connectivity with/without anatomical priors respectively. For the model of effective connectivity with anatomical priors, the best subject discrimination accuracy of SVM was 85.42% with a significance of $P = .009$ (the sensitivity was 87.50% and the specificity was 83.33%), while the best subject discrimination accuracy of SVM was 79.19% with a significance of $P = .013$ (the sensitivity was 75.00% and the specificity was 83.33%) for the model of effective connectivity without anatomical priors. The best results for enriched GCM and normal GCM were both based in SVM.

The highest accuracy of the enriched GCM with anatomical priors in each classifier was higher than that without anatomical priors. Except NBC whose performance was fair, the recognition accuracy of enriched GCM with anatomical priors were high above 70% in all classifiers,

Table 2
Prediction performance of the classifiers based on the model of anatomical connectivity or two models of effective connectivity.

The type of connectivity	Classifier	Classification performance				
		Accuracy	Sensitivity	Specificity	*P*-value	Number of features
Anatomical connectivity	SVM	52.08%	50.00%	54.17%	0.371	2
	KNN	37.50%	33.33%	41.67%	0.422	3
	NMC	43.75%	45.83%	41.67%	0.415	3
	LDA	47.92%	45.83%	50.00%	0.396	3
	NBC	41.67%	41.67%	41.67%	0.483	3
	LR	47.92%	45.83%	50.00%	0.337	2
Effective connectivity without anatomical priors	SVM	79.19%	75.00%	83.33%	0.013	41
	KNN	60.42%	75.00%	45.83%	0.157	28
	NMC	64.58%	70.83%	58.33%	0.135	47
	LDA	72.92%	75.00%	70.83%	0.041	32
	NBC	58.33%	70.83%	41.67%	0.202	40,41
	LR	70.83%	70.83%	70.83%	0.052	34
Effective connectivity with anatomical priors	SVM	85.42%	87.50%	83.33%	0.009	36,37,38
	KNN	70.83%	70.83%	70.83%	0.034	38
	NMC	72.92%	87.50%	58.33%	0.047	29
	LDA	79.19%	75.00%	83.33%	0.027	45
	NBC	64.58%	75.00%	54.17%	0.096	28
	LR	79.19%	75.00%	83.33%	0.024	31,32,33

Accuracy: the proportion of subjects correctly predicted; Sensitivity: the proportion of patients correctly predicted; Specificity: the proportion of controls correctly predicted; Number of features: number of mRMR selected features when achieving the highest prediction accuracy.

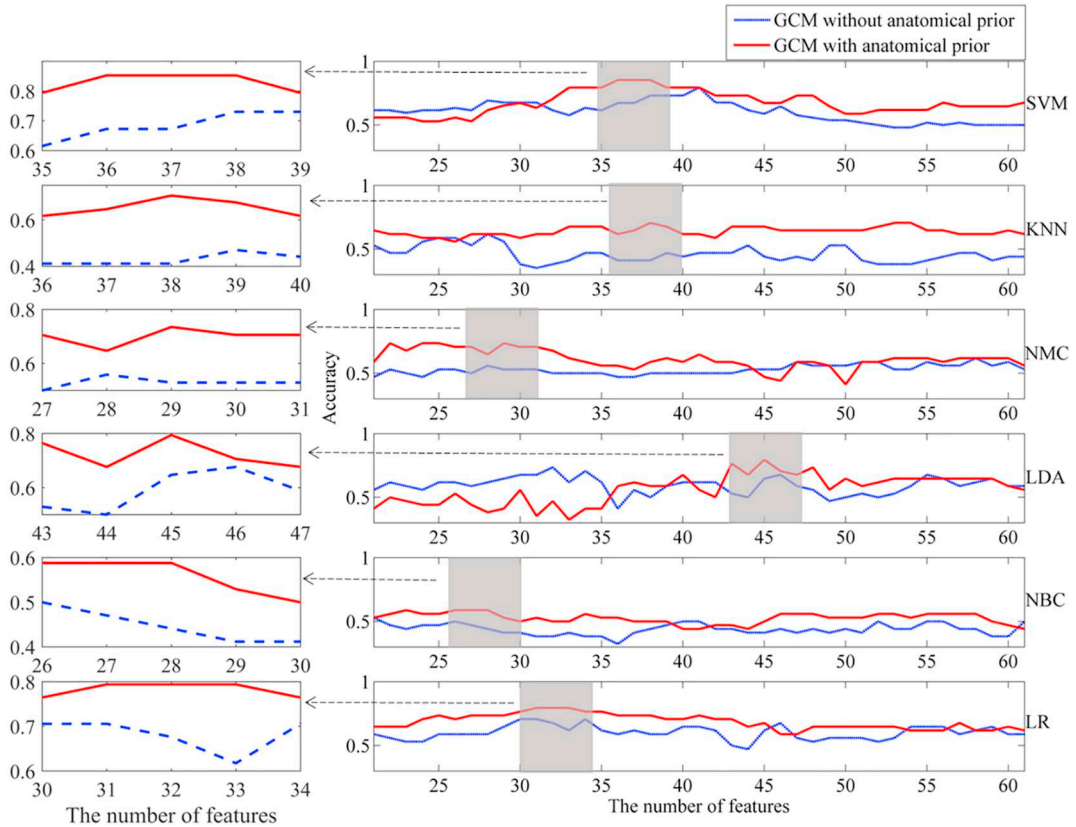

Fig. 2. Classification performance comparison with different number of selected features for two types of GCMs based on different classifiers. The red lines refer to the results of enriched GCM with anatomical priors and the blue lines represent the results of normal GCM. The left subplots were the enlarged details when the classifiers for the enriched GCM with anatomical prior achieved the highest accuracies. (For interpretation of the references to color in this figure legend, the reader is referred to the web version of this article.)

while the accuracy of normal GCM without anatomical priors were just above 60% in all classifiers. In addition, the accuracy of the model of anatomical connectivity was low in all classifiers. The results were summarized in Table 2. Fig. 2 compared the classification performance classifiers with different number setting of selected features, suggesting the superiority of the model of effective connectivity with anatomical priors over that without in anatomical priors in individual recognition.

The normal vector of the classification hyperplane in SVM was used to analysis the contribution rates of discriminating elements. Among them, the most important discriminative features in the enriched GCM with anatomical priors were amygdala to DLPFC during the time period of 120-220 ms with a discriminative vector value being −0.8368 (P = .006) and DLPFC to ACC during the time period of 480-580 ms with a discriminative vector value being 0.8175 (P = .009). In addition,

the significant discriminative feature in the normal GCM without anatomical priors was amygdala to DLPFC during the time period of 120-220 ms with a discriminative vector value being −0.7014 (P = .016).

4. Discussion

The enriched GCM in this study was established to better investigate the dynamic effective connectivity with anatomical priors under sad facial stimuli. Dynamic effective connectivity reflected a dynamical process taking place on anatomical connectivity (Pereda et al., 2005). The results suggested that the enriched algorithm could better distinguish the depression and explore the pathogenesis of depression.

4.1. Transformation model for anatomical information

The results suggested that the strength of the effective connectivity were consistent with the strength of anatomical connectivity. However, the strong functional connectivity might occur between the regions that had weak anatomical connectivity (Stephan et al., 2009). Evidence from empirical studies suggested that the presence of a direct anatomical connection between two brain areas was associated with stronger functional interactions between these two areas (Honey et al., 2007; Hermundstad et al., 2013). It was shown that strong correlation between effective connectivity and anatomical connectivity occurred in the resting-state networks (Greicius et al., 2009). However, the strong effective connectivity could appear between the regions that had no anatomical connectivity (Koch et al., 2002; Stephan et al., 2009; Deco et al., 2013). It was clear that the anatomical connectivity would not predict the brain's functional integration (Ghosh et al., 2008), but it might provide an important constraint (Stephan et al., 2008). The physiological and anatomical studies had shown that anatomical connectivity provided critical constraints on effective connectivity (Deco et al., 2013; Hermundstad et al., 2013; Kaiser, 2013; van Dellen et al., 2013). To summarize, the relation between anatomical and functional connectivity did not follow a simple rule but varied considerably across regions (Koch et al., 2002) as well as could be analyzed within a single mathematical framework (Jbabdi et al., 2007) or simple dynamical systems (Stam et al., 2016) to a certain extent.

4.2. Superiority of the enriched GCM over the normal GCM

The model evidences of normal and enriched GCM both reached minimal when the model order p was set as two, leading to a low model complexity that suitable for effective connectivity estimation contained via three regions. The model evidences of enriched GCM with anatomical priors were significantly smaller than those of normal GCM under any model order setting, suggesting that the model error of enriched GCM was decreased significantly owing to the integration of anatomical priors. The significant decreased model error suggested that the stability and accuracy of enriched GCM was greatly improved, proving the validity and reliability of the enriched algorithm. This assumed that quality of dynamic effective connectivity model should be improved by incorporating anatomical prior knowledge. Such improvement was also demonstrated from the studies elsewhere. Such as, Stephan introduced anatomical connectivity as prior knowledge in dynamic causal model and found that the model was improved by the anatomical connectivity that used to constrain the range of coupling parameters of corresponding regions (Stephan et al., 2009). Also, models for inferring effective connectivity from neuroimaging data have exploited existing knowledge of anatomical connectivity to specify model structure (Stephan et al., 2009; Hermundstad et al., 2013; Kaiser, 2013).

Furthermore, we investigated the effectiveness of the enriched algorithm in depression recognition. The accuracies of all classifiers with anatomical connectivity were low, which suggested that the anatomical connectivity of ROIs could not distinguish the depression well. However, it was clear that the model accuracies with anatomical priors in each classifier were higher than the results without anatomical priors, which suggested that static anatomical connectivity as priors could improve the model of dynamic effective connectivity better. The best accuracies for the enriched GCM and normal GCM were both in SVM, which could solve small sample learning problems better (Xuegong, 2000). The model with effective connectivity within anatomical priors outperformed when distinguishing depression patients from healthy controls. Considering the accuracies of each classifier for the enriched GCM and normal GCM, we suggested that features in the enriched GCM with anatomical priors attributed valuable effort for depression discrimination. This finding had potential implications for improving the diagnosis of depression.

4.3. Effective connectivity with anatomical prior and depression

As the result, it was clear that static anatomical connectivity as priors could improve the diagnosis of depression based on effective connectivity. The effective connectivity represents temporal coherence of brain regions and the anatomical connectivity measures anatomical integrity of white matter tracts, the material backbone for communication between brain regions (Catani et al., 2002). The combination of function and anatomy achieved higher prediction accuracy and enabled individualized prediction in depression (Sui et al., 2014). The study of anatomical connectivity elucidated trait factors underlying brain changes in major depressive disorder (Du et al., 2012). When processing negative stimuli, aberrant functional and anatomical connectivity were reported in subcortical area in depression (Wong et al., 2016). A previous study suggested that the illness led to functional interactions that are more directly related to the underlying anatomical connectivity of the brain (van den Heuvel et al., 2013). In our previous MEG study, the depression could be recognized by functional-structural coupling when the functional connectivity increased rapidly via a dynamic change point detection strategy (Bi et al., 2016). Our finding suggested that the anatomical prior in depression might be attributed to the strength of the effective connectivity, and functional interactions were related to the underlying anatomical connections, which was consistent with our previous study(Bi et al., 2016). The result supported that quantification of the anatomical prior might help better understand the cause of depression and diagnostic indicators.

4.4. Significant discriminative vectors and depression

The discriminative vectors highlighted that the effective connectivity showed the most distinctive characteristics between depression patients and healthy controls. The significant discriminative features in the enriched GCM with anatomical priors were the decreased effective connectivity from amygdala to DLPFC during the time period of 120-220 ms and the increased effective connectivity from DLPFC to ACC during the time period of 480-580 ms in depression. In addition, the significant discriminative feature in the normal GCM without anatomical priors was the decreased effective connectivity from amygdala to DLPFC during the time period of 120-220 ms. The attenuated amygdala-prefrontal functional connectivity or effective connectivity has been reported in depression (Johnstone et al., 2007; Dannlowski et al., 2009; de Almeida et al., 2009; Erk et al., 2010; Philip et al., 2017). Abnormal amygdala activity within 100 ms after stimulus suggested that depression patients might have dysfunctions or negativity biases in perceptual binding of emotional features at very early stage (Liu et al., 2014). We had the same results in depression patients with those reports of the diminished amygdala-prefrontal connectivity (Johnstone et al., 2007; de Almeida et al., 2009; Philip et al., 2017) and corroborated the above mentioned abnormalities. Another significantly enhanced effective connectivity was from DLPFC to ACC in the late stage. In the stages about 500 ms after stimulus onset, accompanying an increase of the connectivity from ACC to prefrontal cortex under sad stimulus, DLPFC would response to ACC's request and make a right

decision to suppress the hyperactivity of amygdala (Yoshimura et al., 2010). However, the powerless DLPFC might not response adequately and caused this enhanced bottom-up information in depression (de Bruijn et al., 2016; Wang et al., 2016). Then, we could suppose that the impaired amygdala-prefrontal effect in early emotional processing might cause the dysfunction in effective connectivity as a circular reaction in depression. The enhanced DLPFC-ACC effect was caused by the powerless DLPFC that failed to suppress the hyperactivity of amygdala in late emotional processing in depression.

The effective connectivity from amygdala to DLPFC in 120-220 ms was found both in the classification of the models with and without anatomical priors, but the effective connectivity from DLPFC to ACC in 480-580 ms was not discovered in the normal GCM without anatomical priors. The decreased effective connectivity of depression in the early rising state of functional connectivity appeared repeatedly as significant discriminative features in two types of GCM. The increased effective connectivity of depression in the late falling state of functional connectivity only appeared in the enriched GCM with anatomical priors. The effective connectivity of depression was lower than that of healthy control in acute rising state of functional connectivity, while the effective connectivity in patients was higher than that of healthy control in acute falling state of functional connectivity. The results might be indicative of more stringent and less dynamic brain function in patients due to the constraint of structure on function in the acute abrupt variation state of functional connectivity, which was consistent with our previous study (Bi et al., 2016). It suggested that the enriched GCM with anatomical priors could be more sensitive than the normal GCM to detect the circuit dysfunction under dynamic functional connectivity exploration.

4.5. Deep brain sources in MEG

The impact of sensor design on depth sensitivity in MEG is often debated. To detect the very small magnetic fields of brain (Vrba and Se, 2001), the superconducting quantum interference device (SQUID) coupled with flux transformers (or pick up coils) was used in an MSR to increase the overall magnetic field sensitivity (Fagaly, 2006). The simulation of MEG activation showed that the simulated MEG fields for subcortical areas were 10 times lower than that for neocortex, but were strong enough to overlap parts of the distribution of the MEG field, especially for the amygdala (Attal et al., 2009; Attal et al., 2012; Attal and Schwartz, 2013). Some studies suggested that under ideal conditions, all sensor types of MEG may be able to detect deeper brain activity, with a slight advantage for axial gradiometers with appropriate baselines in presence of higher noise (Vrba and Se, 2001; da Silva, 2010). Our study used the CTF 275 with first order axial gradiometers in MSR, so it helps detect deeper brain activity better. In addition, head location was monitored to reduce head movement to increase the sensitivity of signals. The limitation of deep source can be overcome by averaging MEG over different trials. So we averaged all trials under sad stimuli for each subject in the preprocessing. The activity of averaged trials in the three regions of interest was shown in supplementary 4. The obvious activities under sad stimuli were found in three regions of interest. In recent several years, there were a lot of MEG studies contained deep brain sources (Hipp et al., 2012; Lu et al., 2013a; Lu et al., 2013b; Nugent et al., 2015; Backus et al., 2016; Bi et al., 2016; Hillebrand et al., 2016; Nugent et al., 2016; Krishnaswamy et al., 2017; Bi et al., 2018; Hall et al., 2018; Pu et al., 2018), especially in depression research (Lu et al., 2013a, Lu et al., 2013b; Nugent et al., 2015; Bi et al., 2016; Nugent et al., 2016; Bi et al., 2018).

5. Conclusion

In this study, the enriched GCM with anatomical priors was provided to better investigate the dynamic effective connectivity under sad facial stimuli and showed a great applicability in exploring between-regions influences. The results suggested that the enriched GCM integrated with the anatomical constraint on function was well. The anatomical constraint on function was useful to explore dynamic functional connectivity. The abnormal anatomical constraint on function occurs in depression, which makes the brain function more stringent and less flexible. The result supported that quantification of the anatomical prior into effective connectivity might help better understand the cause of depression and diagnostic indicators. The proposed approach is sensitive to detect the dynamic dysfunction by the integration of function and anatomy, such as depression, and may also be valuable for other mental diseases.

Role of funding source

The work was supported by the grants of: the National High-tech Research and Development Program of China (2015AA020509); the National Natural Science Foundation of China (81571639, 81371522, and 61372032); the Clinical Medicine Technology Foundation of Jiangsu Province (BL2014009).

Appendix A. Supplementary data

Supplementary data to this article can be found online at https://doi.org/10.1016/j.nicl.2018.11.002.

References

Attal, Y., Schwartz, D., 2013. Assessment of subcortical source localization using deep brain activity imaging model with minimum norm operators: a MEG study. PLoS One 8 (3), e59856.
Attal, Y., Bhattacharjee, M., Yelnik, J., Cottereau, B., Lefèvre, J., Okada, Y., et al., 2009. Modelling and detecting deep brain activity with MEG and EEG. Irbm. 30 (3), 133–138.
Attal, Y., Maess, B., Friederici, A., David, O., 2012. Head models and dynamic causal modeling of subcortical activity using magnetoencephalographic/electroencephalographic data. Rev. Neurosci. 23 (1), 85–95.
Backus, A.R., Schoffelen, J.-M., Szebényi, S., Hanslmayr, S., Doeller, C.F., 2016. Hippocampal-prefrontal theta oscillations support memory integration. Curr. Biol. 26 (4), 450–457.
Bi, K., Hua, L., Wei, M., Qin, J., Lu, Q., Yao, Z., 2016. Dynamic functional–structural coupling within acute functional state change phases: evidence from a depression recognition study. J. Affect. Disord. 191, 145–155.
Bi, K., Chattun, M.R., Liu, X., Wang, Q., Tian, S., Zhang, S., et al., 2018. Abnormal early dynamic individual patterns of functional networks in low gamma band for depression recognition. J. Affect. Disord. 238, 366–374.
Catani, M., Howard, R.J., Pajevic, S., Jones, D.K., 2002. Virtual in vivo interactive dissection of white matter fasciculi in the human brain. NeuroImage 17 (1), 77–94.
Cheng, H., Wang, Y., Sheng, J., et al., 2012. Characteristics and variability of structural networks derived from diffusion tensor imaging. Neuroimage 61 (4), 1153–1164.
Cocchi, L., Harding, I.H., Lord, A., Pantelis, C., Yucel, M., Zalesky, A., 2014. Disruption of structure–function coupling in the schizophrenia connectome. NeuroImage 4, 779–787.
Cribben, I., Haraldsdottir, R., Atlas, L.Y., Wager, T.D., Lindquist, M.A., 2012. Dynamic connectivity regression: determining state-related changes in brain connectivity. NeuroImage 61 (4), 907–920.
da Silva, F.L., 2010. Electrophysiological Basis of MEG Signals. Oxford Univ. Press, London, UK.
Dale, A.M., Liu, A.K., Fischl, B.R., Buckner, R.L., Belliveau, J.W., Lewine, J.D., et al., 2000. Dynamic statistical parametric mapping: combining fMRI and MEG for high-resolution imaging of cortical activity. Neuron 26 (1), 55–67.
Dannlowski, U., Ohrmann, P., Konrad, C., Domschke, K., Bauer, J., Kugel, H., et al., 2009. Reduced amygdala–prefrontal coupling in major depression: association with MAOA genotype and illness severity. Int. J. Neuropsychopharmacol. 12 (01), 11–22.
Davidson, R.J., Pizzagalli, D., Nitschke, J.B., Putnam, K., 2002. Depression: Perspectives from Affective Neuroscience. Annual Review of Psychology. Vol. 53. pp. 545–574.
de Almeida, J.R.C., Versace, A., Mechelli, A., Hassel, S., Quevedo, K., Kupfer, D.J., et al., 2009. Abnormal amygdala-prefrontal effective connectivity to happy faces differentiates bipolar from major depression. Biol. Psychiatry 66 (5), 451.
de Bruijn, A., Möbius, M., Mulders, P., Spijker, J., Tendolkar, I., van Eijndhoven, P., 2016. High Frequency Repetitive Transcranial Magnetic Stimulation of the left DLPFC in Treatment-Resistant Major Depressive Disorder: a Randomized Sham Controlled trial-Preliminary Results of the DREAM study. my. thesisnl.111.
Deco, G., Ponce-Alvarez, A., Mantini, D., Romani, G.L., Hagmann, P., Corbetta, M., 2013. Resting-state functional connectivity emerges from structurally and dynamically shaped slow linear fluctuations. J. Neurosci. 33 (27), 11239–11252.
Ding, C., Peng, H., 2005. Minimum redundancy feature selection from microarray gene expression data. J. Bioinforma. Comput. Biol. 3 (2), 185–205.

Du, M.Y, Wu, Q.Z., Yue, Q., et al., 2012. Voxelwise meta-analysis of gray matter reduction in major depressive disorder. Prog. Neuropsychopharmacol. Biol. Psychiatry 36 (1), 11–16.
Dyrba, M., Grothe, M., Kirste, T., Teipel, S.J., 2015. Multimodal analysis of functional and structural disconnection in Alzheimer's disease using multiple kernel SVM. Hum. Brain Mapp. 36 (6), 2118–2131.
Erk, S., Mikschl, A., Stier, S., Ciaramidaro, A., Gapp, V., Weber, B., et al., 2010. Acute and sustained effects of cognitive emotion regulation in major depression. J. Neurosci. 30 (47), 15726–15734.
Fagaly, R., 2006. Superconducting quantum interference device instruments and applications. Rev. Sci. Instrum. 77 (10), 101101.
Geng, H., Wu, F., Kong, L., Tang, Y., Zhou, Q., Chang, M., et al., 2016. Disrupted structural and functional connectivity in prefrontal-hippocampus circuitry in first-episode medication-naïve adolescent depression. PLoS One 11 (2), e0148345.
Geng, X., Xu, J., Liu, B., Shi, Y., 2018. Multivariate classification of major depressive disorder using the effective connectivity and functional connectivity. Front. Neurosci. 12, 38.
Ghosh, A., Rho, Y., McIntosh, A., Kötter, R., Jirsa, V., 2008. Noise during rest enables the exploration of the brain's dynamic repertoire. PLoS Comput. Biol. 4 (10), e1000196.
Gilbert, J.R., Yarrington, J.S., Wills, K.E., Nugent, A.C., Zarate, C.A., 2018. Glutamatergic signaling drives ketamine-mediated response in depression: evidence from dynamic causal modeling. Int. J. Neuropsychopharmacol. 21 (8), 740–747.
Granger, C.W., 1969. Investigating causal relations by econometric models and cross-spectral methods. Econometrica 424–438.
Granger, C.W., 1980. Testing for causality: a personal viewpoint. J. Econ. Dyn. Control. 2, 329–352.
Greicius, M.D., Supekar, K., Menon, V., Dougherty, R.F., 2009. Resting-state functional connectivity reflects structural connectivity in the default mode network. Cereb. Cortex 19 (1), 72–78.
Hagmann, P., Sporns, O., Madan, N., Cammoun, L., Pienaar, R., Wedeen, V.J., et al., 2010. White matter maturation reshapes structural connectivity in the late developing human brain. Proc. Natl. Acad. Sci. U. S. A. 107 (44), 19067–19072.
Hall, M.B., Nissen, I.A., van Straaten, E.C., Furlong, P.L., Witton, C., Foley, E., et al., 2018. An evaluation of kurtosis beamforming in magnetoencephalography to localize the epileptogenic zone in drug resistant epilepsy patients. Clin. Neurophysiol. 129 (6), 1221–1229.
Henson, R.N., Greve, A., Cooper, E., Gregori, M., Simons, J.S., Geerligs, L., et al., 2016. The effects of hippocampal lesions on MRI measures of structural and functional connectivity. Hippocampus 26 (11), 1447–1463.
Hermundstad, A.M., Bassett, D.S., Brown, K.S., Aminoff, E.M., Clewett, D., Freeman, S., et al., 2013. Structural foundations of resting-state and task-based functional connectivity in the human brain. Proc. Natl. Acad. Sci. 110 (15), 6169–6174.
Hillebrand, A., Nissen, I., Ris-Hilgersom, I., Sijsma, N., Ronner, H., Van Dijk, B., et al., 2016. Detecting epileptiform activity from deeper brain regions in spatially filtered MEG data. Clin. Neurophysiol. 127 (8), 2766–2769.
Hipp, J.F., Hawellek, D.J., Corbetta, M., Siegel, M., Engel, A.K., 2012. Large-scale cortical correlation structure of spontaneous oscillatory activity. Nat. Neurosci. 15 (6), 884.
Honey, C.J., Kötter, R., Breakspear, M., Sporns, O., 2007. Network structure of cerebral cortex shapes functional connectivity on multiple time scales. Proc. Natl. Acad. Sci. 104 (24), 10240–10245.
Hutchison, R.M., Womelsdorf, T., Allen, E.A., Bandettini, P.A., Calhoun, V.D., Corbetta, M., et al., 2013. Dynamic functional connectivity: promise, issues, and interpretations. NeuroImage 80, 360–378.
Jbabdi, S., Woolrich, M., Andersson, J., Behrens, T., 2007. A Bayesian framework for global tractography. NeuroImage 37 (1), 116.
Jenkinson, M., Bannister, P., Brady, M., Smith, S., 2002. Improved optimization for the robust and accurate linear registration and motion correction of brain images. NeuroImage 17 (2), 825–841.
Jensen, O., Hesse, C., 2010. Estimating distributed representations of evoked responses and oscillatory brain activity. In: Hansen, P.C., Kringelbach, M.L., Salmelin, R. (Eds.), MEG Introd. Methods, pp. 156–185.
Johnstone, T., van Reekum, C.M., Urry, H.L., Kalin, N.H., Davidson, R.J., 2007. Failure to regulate: counterproductive recruitment of top-down prefrontal-subcortical circuitry in major depression. J. Neurosci. 27 (33), 8877–8884.
Kaiser, M., 2013. The Potential of the Human Connectome as a Biomarker of Brain Disease.
Kandilarova, S., Stoyanov, D., Kostianev, S., Specht, K., 2018. Altered resting state effective connectivity of anterior insula in Depression. Frontiers in Psychiatry Vol. 9, 83.
Klumpp, H., Fitzgerald, J.M., Kinney, K.L., Kennedy, A.E., Shankman, S.A., Langenecker, S.A., et al., 2017. Predicting cognitive behavioral therapy response in social anxiety disorder with anterior cingulate cortex and amygdala during emotion regulation. NeuroImage 15, 25–34.
Koch, M.A., Dg, Norris, Hund-Georgiadis, M., 2002. An investigation of functional and anatomical connectivity using magnetic resonance imaging. NeuroImage 16 (1), 241–250.
Krishnaswamy, P., Obregon-Henao, G., Ahveninen, J., Khan, S., Babadi, B., Iglesias, J.E., et al., 2017. Sparsity enables estimation of both subcortical and cortical activity from MEG and EEG. In: Proceedings of the National Academy of Sciences, pp. 201705414.
Li, L., Li, B., Bai, Y., Liu, W., Wang, H., Leung, H.C., et al., 2017. Abnormal resting state effective connectivity within the default mode network in major depressive disorder: a spectral dynamic causal modeling study. Brain and Behav. 7 (7), e00732.
Liu, T., Chen, Y., Su, T., Hsieh, J., Chen, L., 2014. Abnormal Early Gamma Responses to Emotional Faces Differentiate Unipolar from Bipolar Disorder Patients. BioMed Research International.
Lu, Q., Li, H., Luo, G., Wang, Y., Tang, H., Han, L., et al., 2012. Impaired prefrontal–amygdala effective connectivity is responsible for the dysfunction of emotion process in major depressive disorder: a dynamic causal modeling study on MEG. Neurosci. Lett. 523 (2), 125–130.
Lu, Q., Bi, K., Liu, C., Luo, G., Tang, H., Yao, Z., 2013a. Predicting depression based on dynamic regional connectivity: a windowed Granger causality analysis of MEG recordings. Brain Res. 1535, 52–60.
Lu, Q., Wang, Y., Luo, G., Li, H., Yao, Z., 2013b. Dynamic connectivity laterality of the amygdala under negative stimulus in depression: a MEG study. Neurosci. Lett. 547, 42–47.
Meng, X., Jiang, R., Lin, D., Bustillo, J., Jones, T., Chen, J., et al., 2017. Predicting individualized clinical measures by a generalized prediction framework and multimodal fusion of MRI data. NeuroImage 145, 218–229.
Moon, T.K., 1996. The expectation-maximization algorithm. In: Signal Processing Magazine. 13. IEEE, pp. 47–60.
Musgrove, D.R., Eberly, L.E., Klimes-Dougan, B., Basgoze, Z., Thomas, K.M., Mueller, B.A., et al., 2015. Impaired bottom-up effective connectivity between amygdala and subgenual anterior cingulate cortex in unmedicated adolescents with major depression: results from a dynamic causal modeling analysis. Brain Connectivity 5 (10), 608–619.
Nugent, A.C., Robinson, S.E., Coppola, R., Furey, M.L., Zarate Jr., C.A., 2015. Group differences in MEG-ICA derived resting state networks: application to major depressive disorder. NeuroImage 118, 1–12.
Nugent, A.C., Robinson, S.E., Coppola, R., Zarate Jr., C.A., 2016. Preliminary differences in resting state MEG functional connectivity pre-and post-ketamine in major depressive disorder. Psychiatry Res. Neuroimaging 2054, 56–66.
Pereda, E., Quiroga, R.Q., Bhattacharya, J., 2005. Nonlinear multivariate analysis of neurophysiological signals. Prog. Neurobiol. 77 (1), 1–37.
Philip, N., Barredo, J., Almeida, J., Tyrka, A., Price, L., Carpenter, L., 2017. 101-network mechanisms of clinical Response to transcranial magnetic stimulation in posttraumatic stress and major depressive disorders. Biol. Psychiatry 81 (10), S42–S43.
Pu, Y., Cheyne, D.O., Cornwell, B.R., Bw, Johnson, 2018. Non-invasive investigation of human hippocampal rhythms using magnetoencephalography: a review. Front. Neurosci. 12, 273.
Roberts, S.J., Penny, W.D., 2002. Variational Bayes for generalized autoregressive models. Signal Processing, IEEE Transactions on. 50 (9), 2245–2257.
Rolls, E.T., Cheng, W., Gilson, M., Qiu, J., Hu, Z., Ruan, H., et al., 2018. Effective connectivity in depression. Biol. Psychiatr. 3 (2), 187–197.
Ruddy, K.L., Leemans, A., Woolley, D.G., Wenderoth, N., Carson, R.G., 2017. Structural and functional cortical connectivity mediating cross education of motor function. J. Neurosci. 37 (10), 2555–2564.
Shew, W.L., Plenz, D., 2013. The functional benefits of criticality in the cortex. Neuroscientist 19 (1), 88–100.
Stam, C., van Straaten, E., Van Dellen, E., Tewarie, P., Gong, G., Hillebrand, A., et al., 2016. The relation between structural and functional connectivity patterns in complex brain networks. Int. J. Psychophysiol. 103, 149–160.
Stephan, K.E., Riera, J.J., Deco, G., Horwitz, B., 2008. The brain connectivity workshops: moving the frontiers of computational systems neuroscience. NeuroImage 42 (1), 1–9.
Stephan, K.E., Tittgemeyer, M., Knösche, T.R., Moran, R.J., Friston, K.J., 2009. Tractography-based priors for dynamic causal models. NeuroImage 47 (4–3), 1628.
Sui, J., Huster, R., Yu, Q., Segall, J.M., Vd, Calhoun, 2014. Function–structure associations of the brain: evidence from multimodal connectivity and covariance studies. NeuroImage 102, 11–23.
Thottakara, P., Lazar, M., Sc, Johnson, Al, Alexander, 2006. Application of Brodmann's area templates for ROI selection in white matter tractography studies. NeuroImage 29 (3), 868–878.
van Dellen, E., Hillebrand, A., Douw, L., Heimans, J.J., Reijneveld, J.C., Stam, C.J., 2013. Local polymorphic delta activity in cortical lesions causes global decreases in functional connectivity. NeuroImage 83, 524–532.
van den Heuvel, M.P., Sporns, O., Collin, G., et al., 2013. Abnormal rich club organization and functional brain dynamics in schizophrenia. JAMA psychiatry 70 (8), 783–792.
Vecchio, F., Miraglia, F., Curcio, G., Altavilla, R., Scrascia, F., Giambattistelli, F., et al., 2016. 20. Cortical brain connectivity evaluated by graph theory in dementia: a correlation study between functional and structural data. Clin. Neurophysiol. 127 (4), e137.
Vrba, J., Se, Robinson, 2001. Signal processing in magnetoencephalography. Methods 25 (2), 249–271.
Wackerhagen, C., Wüstenberg, T., Mohnke, S., Erk, S., Veer, I.M., Kruschwitz, J.D., et al., 2017. Influence of familial risk for depression on cortico-limbic connectivity during implicit emotional processing. Neuropsychopharmacology 42 (8), 1729.
Wang, Y.-L., S-Z, Yang, W-L, Sun, Y-Z, Shi, Duan, H.-F., 2016. Altered functional interaction hub between affective network and cognitive control network in patients with major depressive disorder. Behav. Brain Res. 298, 301–309.
Wong, N., Liu, H.-L., Lin, C., Huang, C.-M., Wai, Y.-Y., Lee, S.-H., et al., 2016. Loneliness in late-life depression: structural and functional connectivity during affective processing. Psychol. Med. 46 (12), 2485–2499.
Xuegong, Z., 2000. Introduction to statistical learning theory and support vector machines. Acta Automat. Sin. 26 (1), 32–42.

Yin, Y., He, X., Xu, M., Hou, Z., Song, X., Sui, Y., et al., 2016. Structural and functional connectivity of default mode network underlying the cognitive impairment in late-onset depression. Sci. Rep. 6.

Yoshimura, S., Okamoto, Y., Onoda, K., Matsunaga, M., Ueda, K., Suzuki, S.-i., et al., 2010. Rostral anterior cingulate cortex activity mediates the relationship between the depressive symptoms and the medial prefrontal cortex activity. J. Affect. Disord. 122 (1–2), 76–85.

Zhang, Z., Liao, W., Chen, H., Mantini, D., Ding, J.R., Xu, Q., et al., 2011. Altered functional-structural coupling of large-scale brain networks in idiopathic generalized epilepsy. Brain 134 (10), 2912–2928.

Zheng, L.J., Yang, G.F., Zhang, X.Y., Wang, Y.F., Liu, Y., Zheng, G., et al., 2017. Altered amygdala and hippocampus effective connectivity in mild cognitive impairment patients with depression: a resting-state functional MR imaging study with granger causality analysis. Oncotarget 8 (15), 25021.

Zhigalov, A., Arnulfo, G., Nobili, L., Palva, S., Palva, J.M., 2017. Modular co-organization of functional connectivity and scale-free dynamics in the human brain. Network Neurosci. 1 (2), 143–165.